Improving Radar Refractivity Retrieval by Considering the Change in the Refractivity Profile and the Varying Altitudes of Ground Targets

YA-CHIEN FENG AND FRÉDÉRIC FABRY

Department of Atmospheric and Oceanic Sciences, McGill University, Montreal, Quebec, Canada

TAMMY M. WECKWERTH

Earth Observing Laboratory, National Center for Atmospheric Research, Boulder, Colorado*

(Manuscript received 3 November 2015, in final form 24 February 2016)

ABSTRACT

Accurate radar refractivity retrievals are critical for quantitative applications, such as assimilating refractivity into numerical models or studying boundary layer and convection processes. However, the technique as originally developed makes some simplistic assumptions about the heights of ground targets (H_T) and the vertical gradient of refractivity (dN/dh). In reality, the field of target phases used for refractivity retrieval is noisy because of varying terrain and introduces estimation biases. To obtain a refractivity map at a constant height above terrain, a 2D horizontal refractivity field at the radar height must be computed and corrected for altitude using an average dN/dh. This is achieved by theoretically clarifying the interpretation of the measured phase considering the varying H_T and the temporal change of dN/dh. Evolving dN/dh causes systematic refractivity biases, as it affects the beam trajectory, the associated target range, and the refractivity field sampled between selected targets of different heights. To determine H_T and dN/dh changes, a twofold approach is proposed: first, H_T can be reasonably inferred based on terrain height; then, a new method of dN/dh estimation is devised by using the property of the returned powers of a pointlike target at successive antenna elevations. The dN/dh obtained shows skill based on in situ tower observation. As a result, the data quality of the retrieved refractivity may be improved with the newly added information of dN/dh and H_T.

1. Introduction and motivation

High-resolution near-surface moisture is crucial to pursue knowledge of convective and boundary layer processes (Weckwerth et al. 1999; Weckwerth 2000; Sherwood et al. 2010). From numerical model simulations and data analysis, convection initiation and quantitative precipitation forecasting are shown to be sensitive to accurate measurements of moisture and temperature variability at the surface and in the boundary layer (e.g., Zawadzki et al. 1981; Crook 1996; Weckwerth et al. 1999). However, moisture observations at high temporal and spatial resolutions in the lower boundary layer are not readily available. The lack of information on moisture is one of the main limitations of mesoscale short-term forecasting (Emanuel et al. 1995; Dabberdt and Schlatter 1996; Fabry and Sun 2010; Hanley et al. 2011).

Fabry et al. (1997) proposed a method to measure the refractivity (N) of near-surface air by using weather radars and fixed ground targets. This approach provides insight into small-scale low-level horizontal humidity variations through the retrieved refractivity map by radars, and it may partially fill the observational data gap in the lower boundary layer. Refractivity, $N = (n - 1) \times 10^6$, is used for convenience to show the variation of the refractive index (n). Refractivity is a function of pressure P (hPa), temperature T (K), and water vapor pressure e (hPa). At microwave frequencies, the empirical approximation of refractivity is (Smith and Weintraub 1953)

* The National Center for Atmospheric Research is sponsored by the National Science Foundation.

Corresponding author address: Ya-Chien Feng, Dept. of Atmospheric and Oceanic Sciences, McGill University, 805 Sherbrooke St. W., Montreal QC H3A 0B9, Canada.
E-mail: ya-chien.feng@mail.mcgill.ca

DOI: 10.1175/JTECH-D-15-0224.1

$$N \simeq 77.6\frac{P}{T} + 373\,000\frac{e}{T^2}. \quad (1)$$

Refractivity is more sensitive to moisture variation; for example, changes of 1°C in temperature or 0.2 hPa in vapor pressure (e.g., 0.2°C in dewpoint temperature at 18°C) result in 1 unit of refractivity change. Fabry (2006) further noted that the variation of water vapor is the main source of the spatial variability of refractivity in summerlike conditions.

Comparisons between refractivity measured by the radar and other instruments in the boundary layer show high correlations in time and space (Fabry et al. 1997; Weckwerth et al. 2005; Bodine et al. 2011). Since high-temporal- (about 5–10 min) and high-spatial- (4 km by 4 km in the horizontal after smoothing) resolution refractivity retrievals have been obtained, many studies have demonstrated the potential utility of refractivity maps for studying near-surface moisture variation associated with a variety of weather phenomena, such as convection initiation, convection evolution, and characteristics of the boundary layer (Weckwerth et al. 2005; Fabry 2006; Buban et al. 2007; Chen et al. 2007; Roberts et al. 2008; Koch et al. 2008; Besson et al. 2012; Nicol et al. 2014). Refractivity maps not only provide small-scale moisture variability particularly in those areas without a dense mesonet but also show boundaries prior to the fine line of traditional reflectivity (Weckwerth et al. 2005; Heinselman et al. 2009; Wakimoto and Murphey 2010; Bodine et al. 2011). However, the coverage range of refractivity data is about 40–60 km, dictated by the topography and radio wave propagation. The range up to which refractivity data can be collected is limited; to go beyond, a radar network is needed. Thus, a networked technique has been developed for merging multiple X-band radars to extend the coverage of refractivity observations (Hao et al. 2006; Fritz and Chandrasekar 2009).

Montmerle et al. (2002) and Sun (2005) assimilated radar refractivity information to adjust the quantity and distribution of low-level moisture. The newly added information not only modified the low-level humidity field but also changed the spatial variability of moisture, which enhanced the intensity of the storm, leading to better quantitative precipitation forecasting. As a result, the research community has been preparing to assimilate the composite refractivity data from operational radar networks to numerical models in order to improve short-term forecasting skill (Besson et al. 2012; Caumont et al. 2013; Gasperoni et al. 2013; Nicol et al. 2013; Nicol and Illingworth 2013; Nicol et al. 2014).

For such quantitative applications, the accuracy of the refractivity retrieval is important and thus it is critical to gain more knowledge about the biases and the representativeness of the retrieval. Although the quality of the retrieval has been discussed from different aspects and improved in the last decade (Fabry 2004; Park and Fabry 2010; Besson et al. 2012; Parent du Chatelet et al. 2012; Caumont et al. 2013; Nicol et al. 2013; Nicol and Illingworth 2013), the unsolved problem associated with the vertical gradient of refractivity (dN/dh) and uneven target heights (H_T) remains challenging. A consequence of these issues is the difficulties of assigning a height to the retrieved refractivity fields and the prominent diurnal periodicity of the refractivity difference between in situ observations and the radar estimations (Fabry 2004; Weckwerth et al. 2005; Bodine et al. 2011). The net result is that the refractivity retrieval is representative of conditions over different heights; for example, it can represent the lower 250 m of the boundary layer when the convective boundary layer is well mixed in summer daytime conditions but a much shallower layer in the nighttime (Weckwerth et al. 2005).

The goal of this research is to rethink refractivity retrieval to obtain a more accurate near-surface 2D horizontal refractivity map at a given representative height and additional information on dN/dh. In section 2 the assumptions in the original method are revisited, and the refractivity biases associated with the H_T and dN/dh are clarified and quantified. Then, a new method for estimating the representative H_T and dN/dh by using echo strength variations of ground targets is introduced in section 3. The estimated dN/dh from the radar and targets is compared with in situ observation in section 4. In the last section, the improvements and limits of the retrieval method are summarized by applying the newly obtained information.

2. Phase difference and refractivity

a. *The basis of radar refractivity retrieval*

The concept of radar refractivity retrieval is based on the varying time t_{travel} that electromagnetic waves travel back and forth between the radar and a ground target. The time is affected by the refractive index along its propagating path and can be expressed as

$$t_{\text{travel}} = 2r\frac{n}{c}, \quad (2)$$

where r is the one-way beam path range from the radar to the target and c is the speed of light in vacuum. Fabry et al. (1997) used the phase of a fixed ground target as a proxy for the time. Given a stable radar transmitter frequency (f), the radar-measured phase (ϕ) of a

stationary point ground target depends on the time taken by a radar pulse for a two-way path:

$$\phi(r) = 2\pi f t_{\text{travel}} = \frac{4\pi f}{10^6 c}\int_0^r N(r',t)\,dr'. \quad (3)$$

The observed phase largely exceeds 2π, while the phase measurement is aliased within $\pm\pi$. To mitigate somewhat this problem of phase aliasing, the phase difference ($\Delta\phi$) of a stationary ground target between a scan at time t and at a reference time t_{ref} can provide the information of the path-averaged refractivity variation:

$$\Delta\phi = \phi_t - \phi_{t_{\text{ref}}} = \frac{4\pi f}{10^6 c}\int_0^r [N(r',t) - N(r',t_{\text{ref}})]\,dr'. \quad (4)$$

The reference phase ($\phi_{t_{\text{ref}}}$) is determined, while the refractivity field is assumed to be nearly horizontally uniform with a known refractivity at t_{ref}, which is usually during or after stratiform rain in windy and cool conditions. Based on (4), the average change of refractivity along the beam path, $\overline{\Delta N} = \overline{N(t)} - \overline{N(t_{\text{ref}})}$, can be derived from the radial gradient of phase difference, $d\Delta\phi/dr$. From these measurements, small-scale variations of refractivity among the reliable fixed ground targets can be estimated from the slope of phase difference between the neighboring target pairs. For example, the local refractivity variation between targets T_1 and T_2 on the same azimuth is proportional to the gradient of the phase difference between these targets, $(\Delta\phi_{T_2} - \Delta\phi_{T_1})/(r_{T_2} - r_{T_1})$. Consequently, the refractivity value can be obtained by adding the refractivity change field to the known reference refractivity field.

b. *Revisiting the assumptions and unsolved problems*

The accuracy of retrieved refractivity critically depends on the quality of the phase differences of reliable ground targets. Phase differences caused by reasons other than the real atmospheric refractivity variations lead to noisiness in $\Delta\phi$ fields and bias in the refractivity retrievals. Therefore, quantifying the noise in $\Delta\phi$ introduced by different sources of uncertainties will enable improvements to the current retrieval algorithm. Possible sources leading to poorer refractivity estimates are discussed in many works and fall into the following three categories: 1) target uncertainty in its stability, height, and location (Fabry et al. 1997; Fabry 2004; Besson et al. 2012; Nicol and Illingworth 2013; Nicol et al. 2013); 2) propagation conditions associated with dN/dh and height difference between the radar and ground targets (Fabry 2004; Park and Fabry 2010; Bodine et al. 2011); and 3) drifts in the transmitter frequency (Parent du Chatelet et al. 2012; Nicol et al. 2013). Here, the focus is on the most basic unsolved part: the effects of atmospheric propagation conditions and the height differences between the radar and the targets.

The simplistic assumptions that were originally made by Fabry et al. (1997) to obtain a 2D refractivity field are as follows: 1) the heights of selected targets and the radar antenna height are identical ($H_T = H_R$); 2) the earth's curvature is neglected; or alternatively, dN/dh is $-157\,\text{km}^{-1}$ everywhere; and 3) the reference refractivity map is uniform and constant. Yet, these conditions are generally not realistic: real targets are at various heights, such as on hilly terrain or in an urban area, while dN/dh evolves diurnally and changes significantly with weather conditions, affecting the propagation of radar beam path and r. Consequently, r cannot be considered constant.

As a result, since targets are at different heights under varying dN/dh conditions, the field of measured phase difference between nearby pairs of targets is noisy. A noisy phase difference field makes dealiasing and the estimation of small-area radial gradients of $\Delta\phi$ more difficult, lowering the quality of the refractivity retrieval, particularly for short-wavelength radars and for targets at far ranges. To limit this problem, in postprocessing, the noisy phase differences are generally smoothed by either a pyramidal weighting function over a 4 km by 4 km area or a least squares fit (Fabry 2004; Hao et al. 2006; Nicol et al. 2013). The smoothing process washes out the unrealistic sudden local refractivity change due to the noisy $\Delta\phi$ problem. Caumont et al. (2013) also suggested a new weighting parameter for extracting meaningful signal and smoothing the noisiness of retrieved refractivity change. Nonetheless, the smoothing process reduces the spatial resolution of the data and does not fully resolve the incorrect physical biases introduced by dN/dh and target height variability.

c. *Reinterpretation of the measured* $\Delta\phi$

The observed phase is affected by the horizontal and vertical variations of refractivity along the radar beam path from the radar to the ground target. Park and Fabry (2010) developed a simulator to explore the observed noisy phase difference by considering the temporal change of vertical variation of refractivity and the height difference between targets and the radar. The temporal phase difference of a point target at t and t_{ref} is expressed as

$$\Delta\phi = \frac{4\pi f}{10^6 c}\left\{\underbrace{\overline{N(t)}r - \overline{N(t_{\rm ref})}r_{\rm ref}}_{\rm (i)} + \underbrace{(H_T - H_R)\left[\frac{dN}{dh}\frac{r}{2} - \left(\frac{dN}{dh}\right)_{\rm ref}\frac{r_{\rm ref}}{2}\right]}_{\rm (ii)}\right.$$
$$\left.\underbrace{-\left[\frac{dN}{dh}\left(\frac{1+(a+H_R)\frac{1}{10^6}\left(\frac{dN}{dh}\right)}{12(a+H_R)}\right)r^3 - \left(\frac{dN}{dh}\right)_{\rm ref}\left(\frac{1+(a+H_R)\frac{1}{10^6}\left(\frac{dN}{dh}\right)_{\rm ref}}{12(a+H_R)}\right)r_{\rm ref}^3\right]}_{\rm (iii)}\right\}, \quad (5)$$

with a being the radius of the earth, and H_T and H_R being the representative heights of the target and the radar above sea level, respectively. The phase change in time of a ground target records the information of (i) the change of refractivity in the horizontal at the radar height, (ii) the change of refractivity with height associated with the height difference between the radar and the target, and (iii) the ray curvature relative to the curvature of the earth. This equation theoretically describes the causes of measured $\Delta\phi$, assuming a single homogeneous dN/dh at a particular time. It illustrates that the phase varies not only as a result of refractivity change along the path but also because the path range (r) to the target changes when dN/dh varies. If dN/dh varies along the beam path, then there is no simple analytic formulation for $\Delta\phi$, and the contribution of the changing trajectory to $\Delta\phi$ must be determined by iterations.

Furthermore, the path range is affected by the atmospheric propagation condition and the location of the target, and can be expressed as (Park and Fabry 2010)

$$r = \left|\frac{dn}{dh}\right|^{-1}\cos^{-1}\left[1 - \frac{C\left(\frac{dn}{dh}\right)^2}{2}\right], \quad \text{with} \quad (6)$$
$$C = (a+H_R)^2 + (a+H_T)^2 - 2(a+H_R)(a+H_T)\cos\left[\frac{D}{(a+H_R)}\right],$$

where D is the arc distance to the target at the radar height parallel to the sea level surface. Recall that dn/dh equals $10^{-6}dN/dh$. The path range hence varies with dN/dh and also depends on the varying height and distance of targets, making (5) more complicated than (4), which was used previously.

To further clarify the causes of $\Delta\phi$ in (5), we separate r into three terms: the arc distance (D) to the target at the radar height; the range variation Δr_1 resulting from the height difference between H_T and H_R given $dN/dh = -157\ \mathrm{km}^{-1}$; and the range variation Δr_2 related to the change in the path given a change in dN/dh, as well as independent of H_T:

$$r = D + \Delta r_1\left[D, H_T - H_R, \left(\frac{dN}{dh}\right)_{-157}\right] + \Delta r_2\left[D, \frac{dN}{dh} - \left(\frac{dN}{dh}\right)_{-157}\right]. \quad (7)$$

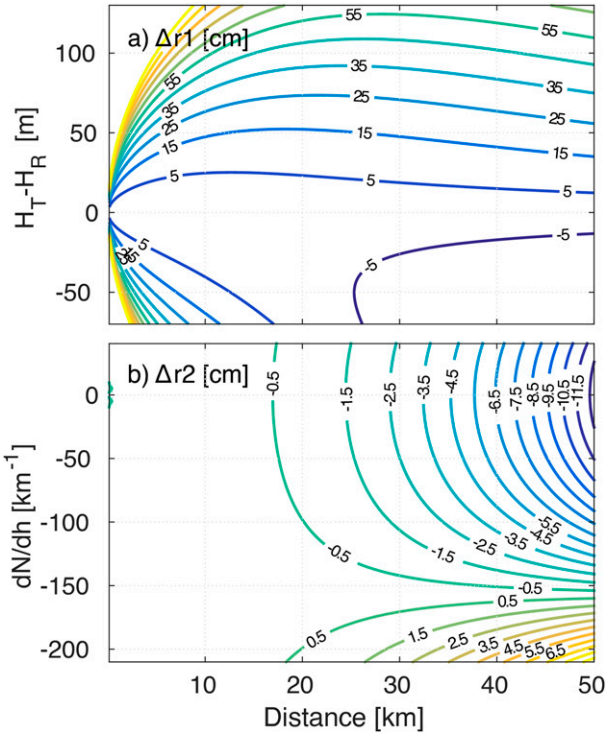

FIG. 1. Additional contributions to target ranges caused by target heights H_T and propagation conditions dN/dh (km^{-1}). (a) Range variation Δr_1 (cm) as a function of the arc distance D of ground targets and the height difference between the ground target and the radar ($H_T - H_R$). (b) Range change Δr_2 (cm) caused by dN/dh changes with respect to $dN/dh_{\rm ref} = -157\ \mathrm{km}^{-1}$.

Consequently, the range variation can be separated into the effects of differing target heights and of varying $\Delta(dN/dh)$. Figure 1 demonstrates that Δr_1 is of the order of tens of centimeters, and Δr_2 is typically a few centimeters, both sufficient to change the target phase considerably.

The phase difference in (5) can be revised by substituting r from (7) and by neglecting small terms of phase differences using a scale analysis under extreme conditions ($|\Delta\phi| < 1°$ at radar frequencies up to X-band given D up to 50 km, $\Delta(dN/dh)$ up to 200 km^{-1}, and $H_T - H_R$ up to 100 m):

$$\Delta\phi = \frac{4\pi f}{10^6 c} \times \left\{ \underbrace{D[\overline{N(t)} - \overline{N(t_{\text{ref}})}]}_{\text{(i) horizontal } \overline{\Delta N} \text{ at } H_R} + \underbrace{\overline{N(t_{\text{ref}})}(\Delta r_2 - \Delta r_{2\text{ref}})}_{\text{(ii) bias: propagation effect (range)}} + \underbrace{\frac{D(H_T - H_R)}{2}\left[\frac{dN}{dh} - \left(\frac{dN}{dh}\right)_{\text{ref}}\right]}_{\text{(iii) bias: target height effect}} \right.$$
$$\left. \underbrace{-D^3\left\{\frac{dN}{dh}\left[\frac{1 + (a + H_R)\frac{1}{10^6}\left(\frac{dN}{dh}\right)}{12(a + H_R)}\right] - \left(\frac{dN}{dh}\right)_{\text{ref}}\left[\frac{1 + (a + H_R)\frac{1}{10^6}\left(\frac{dN}{dh}\right)_{\text{ref}}}{12(a + H_R)}\right]\right\}}_{\text{(iv) bias: propagation effect (changing beam curvature)}} \right\} \quad (8)$$

Using (8), the various contributions to the phase change $\Delta\phi$ can be discussed and analyzed in greater detail.

The average change of the horizontal refractivity at the radar height ($\overline{\Delta N}_{H_R}$), term (i) in (8), is the original term from Fabry et al. (1997). The radial gradient of $\Delta\phi$ of this term is used to obtain a refractivity map at the radar height. In addition, (8) clarifies the misleading concept of the (i) term in (5), because it represents not only the $\overline{\Delta N}_{H_R}$, but also the range variation Δr_2 due to the propagation effect, term (ii) in (8). The result of the scale analysis also shows that the effect of range variations associated with H_T (Δr_1) can be neglected, because Δr_1 does not change with dN/dh, and $\Delta\phi$ caused by $\Delta r_1[N(t) - N(t_{\text{ref}})]$ is smaller than 1°. Furthermore, other $\Delta\phi$ terms in (8) caused by the effects of variable target heights and the vertical gradient of refractivity result in biases of average refractivity along the

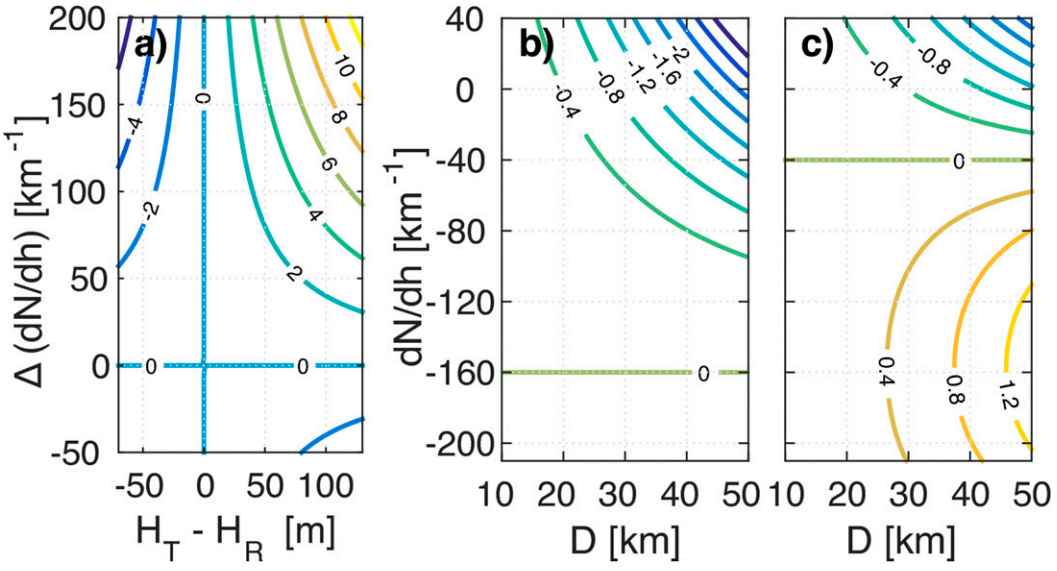

FIG. 2. (a) Average refractivity bias $\overline{N_{\text{bias}}}$ along the beam path due to target height effects as a function of the height difference between the radar and the target, as well as of the atmospheric vertical refractivity profile difference $\Delta(dN/dh) = dN/dh - (dN/dh)_{\text{ref}}$. This $\overline{N_{\text{bias}}}$ is calculated based on term (iii) in (8). (b) $\overline{N_{\text{bias}}}$ related to the change of the beam trajectory defined as terms (ii) and (iv) in (8) as a function of the distance to the ground target and dN/dh conditions. Note that this bias also depends on the dN/dh_{ref}, set here as -157 km^{-1}. (c) The $\overline{N_{\text{bias}}}$ caused by the same effect as (b), but with $dN/dh_{\text{ref}} = -40$ km^{-1}.

beam path $\overline{N_{\text{bias}}}$ in the original refractivity retrieval. Term $\overline{N_{\text{bias}}}$ can be expressed by $(10^6 c/4\pi) \times (\Delta\phi/D)$. If H_T and dN/dh can be retrieved using a yet unspecified method, then those terms can be accounted for and removed, resulting in a ΔN field that is related only to the horizontal variation of refractivity at H_R.

The temporal variation of the vertical refractivity profile is a source of bias for $\overline{\Delta N}_{H_R}$. Figure 2a shows the magnitude of the refractivity bias as a function of the vertical refractivity profile for targets at different heights from H_R, which is calculated from term (iii) in (8). For example, when $\Delta(dN/dh)$ changes by $150\,\text{km}^{-1}$, the resulting $\overline{N_{\text{bias}}}$ is 2 N-units for a radar and a target 25 m apart in altitude. The term "N unit" expresses the fact that the change or bias applies to N, not to another unitless quantity. Moreover, the observed phase is affected by both the beam path range variation (Δr_2) and the varying propagation conditions the radar ray experiences along these changing paths, that is, terms (ii) and (iv) in (8). Term $\overline{N_{\text{bias}}}$ due to these propagation effects is a function of dN/dh, dN/dh_{ref}, and the distance to the targets. Figures 2b and 2c show how $\overline{N_{\text{bias}}}$ changes with propagation conditions for dN/dh_{ref} of -157 and $-40\,\text{km}^{-1}$, respectively. For geometry purposes, $dN/dh_{\text{ref}} = -157\,\text{km}^{-1}$ is used to help clarify the many contributions to range, where Δr_2 then corresponds to the pathlength added by propagation; from the meteorological point of view, $dN/dh_{\text{ref}} = -40\,\text{km}^{-1}$ represents the normal refraction when the near surface is under well-mixed conditions and is the dN/dh_{ref} usually used in the retrieval technique. The magnitudes of $\overline{N_{\text{bias}}}$ in different dN/dh_{ref} conditions are similar and are all proportional to the variation of dN/dh and target distance, but they are relatively smaller than the $\overline{N_{\text{bias}}}$ caused by the height effect discussed previously. For instance in Fig. 2b, when $\Delta(dN/dh)$ changes from -160 to $-40\,\text{km}^{-1}$, $\overline{N_{\text{bias}}}$ of the target 25 km away from the radar is about -0.4 N-units.

d. Noisy $\Delta\phi$ and local N biases

All of the discussion until now focused on biases in N averaged between the radar and a target. Finer resolution of refractivity change is gained from the phase difference between neighboring targets along the same azimuth. However, the targets at different heights or on varying terrain introduce noisiness in $\Delta\phi$ and biases in the refractivity estimated from these $\Delta\phi$. The temporally averaged refractivity change between a target pair, T_2 and T_1, derived from the phase difference gradient between targets is such that

$$\Delta N_{T_2-T_1} = \frac{\Delta\phi_{T_2} - \Delta\phi_{T_1}}{\frac{4\pi f}{10^6 c}\Delta D} = \underbrace{\Delta\overline{N(t)}_{T_2-T_1}}_{\text{(i) horizontal } \Delta N \text{ at } H_R} + \underbrace{\frac{1}{2}\left(\Delta\frac{dN}{dh}\right)\left(\frac{H_{T_1}+H_{T_2}}{2} - H_R\right)}_{\text{(ii) } \Delta H \text{ and } \Delta dN/dh}$$
$$+ \underbrace{\frac{1}{2}\left(\Delta\frac{dN}{dh}\right)\left(\frac{D_{T_1}+\frac{\Delta D}{2}}{\Delta D}\right)(H_{T_2} - H_{T_1})}_{\text{(iii) bias: target height effect}} + \underbrace{\frac{1}{\Delta D}\overline{N(t_{\text{ref}})}[(\Delta r_{2T_2} - \Delta r_{2\text{ref}T_2}) - (\Delta r_{2T_1} - \Delta r_{2\text{ref}T_1})]}_{\text{(iv) bias: propagation effect (range)}}$$
$$- \underbrace{(D_{T_2}^2 + D_{T_1}D_{T_2} + D_{T_1}^2)\left\{\frac{dN}{dh}\left[\frac{1+(a+H_R)\frac{1}{10^6}\left(\frac{dN}{dh}\right)}{12(a+H_R)}\right] - \left(\frac{dN}{dh}\right)_{\text{ref}}\left[\frac{1+(a+H_R)\frac{1}{10^6}\left(\frac{dN}{dh}\right)_{\text{ref}}}{12(a+H_R)}\right]\right\}}_{\text{(v) bias: propagation effect (changing beam curvature)}}, \quad (9)$$

where ΔD is the arc distance between the target pair $(D_{T_2} - D_{T_1})$ at the radar height. This key equation clarifies the goal and the problems of the refractivity retrieval method in more detail and will be used to improve the original refractivity retrieval.

1) N AT A GIVEN HEIGHT ABOVE TERRAIN

To quantitatively interpret and apply the refractivity retrieval, one generally wants to estimate the refractivity field at a given height above the terrain. The temporal change of refractivity between targets combines the 2D refractivity change at the radar height and the change of the vertical refractivity difference between the radar and the average height of targets, which are terms (i) and (ii) in (9). However, there are some more residual terms of $\Delta\phi$ that introduce biases in the refractivity. These systematic biases are associated with the evolving dN/dh and the height difference between target pairs. Two aspects of

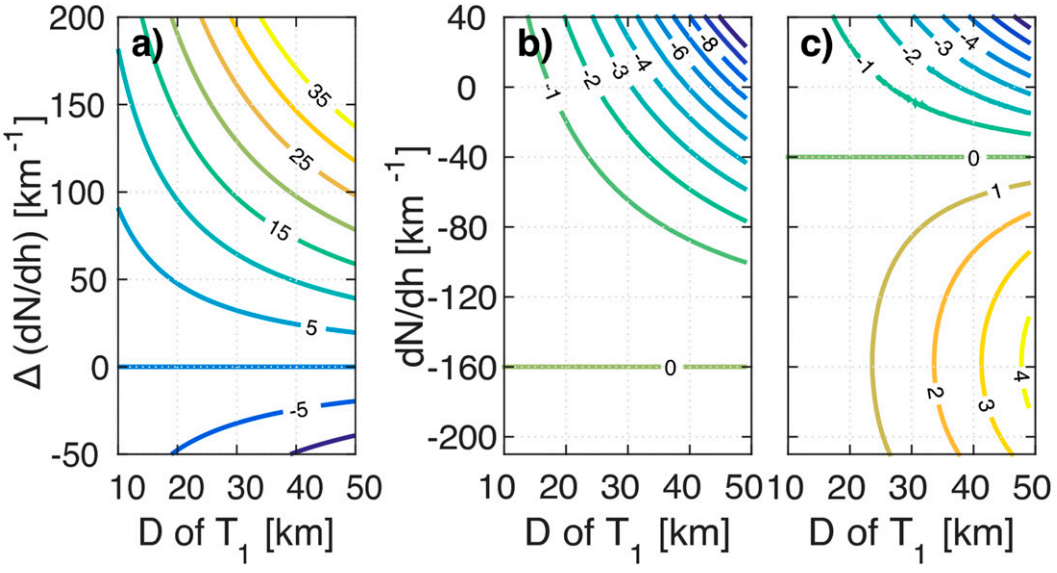

FIG. 3. (a) Local refractivity bias due to the effect of the height difference between a pair of neighboring ground targets (T_1 and T_2) 10 m apart in height and 1 km apart in distance. This bias is calculated from term (iii) in (9) as a function of distance of T_1 and $\Delta(dN/dh)$. (b) Local N bias associated with the beam propagation effect, which causes pathlength variations and beam curvature changes, i.e., terms (iv) and (v) in (9), respectively. Note this local N bias is calculated when $N/dh_{\text{ref}} = -157\,\text{km}^{-1}$. (c) As in (b), but with $dN/dh_{\text{ref}} = -40\,\text{km}^{-1}$.

biases are discussed and quantified: the effects of the difference of target heights and the beam trajectory. Both of these biases are proportional to $\Delta(dN/dh)$ and to the distance of targets from the radar.

2) LOCAL N BIAS DUE TO TARGET HEIGHT

The measured $\Delta\phi$ field is biased by the variability of heights of neighboring ground targets. Even with small height differences and small dN/dh changes, the local N bias of refractivity is significant. According to term (iii) in (9), the magnitude of the bias due to the target's height effect can reach tens of N-units (Fig. 3a). For targets at around 20 km in range and given $\Delta(dN/dh) = 100\,\text{km}^{-1}$, a typical summertime diurnal variation of $\Delta(dN/dh)$, an extra $\Delta\phi = 72°$ is measured at S band for targets that are separated by $\Delta H = 10$ m and $\Delta D = 1$ km. The extra $\Delta\phi$ consequently causes a 10 N-units bias locally. This large bias reflects how strongly height differences between targets affect the local N bias (noisy $\Delta\phi$) when dN/dh changes. This is a serious concern because it is common to have targets or terrain of varying heights along any given azimuth.

3) LOCAL N BIAS DUE TO THE PROPAGATION EFFECT

The evolving propagation condition (dN/dh) affects the pathlength variation and the changing beam curvature relative to the earth's curvature, as terms (iv) and (v) show in (9), respectively. Hence, this local N bias depends on Δr_2 and dN/dh_{ref}. Figures 3b and 3c show the similar relationship of local N bias associated with different dN/dh_{ref}, -157 and $-40\,\text{km}^{-1}$, respectively. Figure 3b shows that this local refractivity bias is of the order of -1 N-unit in the case of two targets 1 km apart at 20 km with $\Delta(dN/dh) = 150\,\text{km}^{-1}$. The local N bias among nearby target pairs is higher compared with the previously discussed averaged bias along the beam path (Fig. 2b). This is because the amplification introduced by the computation of range derivatives of $\Delta\phi$ results in a larger ΔN bias.

4) CONSEQUENCES

The biases discussed above show how the data quality of retrieved refractivity is strongly affected by the diurnal evolving dN/dh. On the other hand, the temporal phase difference, say $\Delta\phi = \phi_{t+30\text{min}} - \phi_t$, is less noisy due to a smaller $\Delta(dN/dh)$ within a short time than the phase differences computed over several days. A 2D ΔN map derived from $\Delta\phi$ in a short time period is useful to track the moving boundary of the thermodynamic variations. For quantitative applications, however, the N field is easier to interpret and is directly related to (1). Thus, the problem of noisy $\Delta\phi$ observed when large change in dN/dh occurs cannot be entirely avoided.

In addition, the result of N estimation is very sensitive to the size of the smoothing window or of the $\Delta\phi$ regression computation to obtain the slope of ΔN. A small smoothing window with a limited number of targets

causes larger uncertainty due to fewer constraints. If a small window containing noisy $\Delta\phi$ is selected, the ΔN computed will have a radial wavy pattern and the resulting bias of ΔN easily becomes larger, roughly proportional to $(\Delta D)^{-3/2}$. On the contrary, if the smoothing window is too large, then the small spatial structure of N is smoothed out. The smoothing window should be determined considering the variability of $\Delta\phi$, which is related to the variability of target heights, the small-scale horizontal variation of N, azimuth alignments of targets, and the number of targets available. The setup of the smoothing window and the representative spatial resolution of N estimates is a problem that deserves a more thorough study than can be done here.

Previous work uses smoothing to reduce the noisy $\Delta\phi$ between neighboring targets in order to obtain a reasonable refractivity field, only mitigating part of the problem. The goal of obtaining a refractivity map at a given known height requires accounting for biases due to propagation conditions and target heights. However, the lack of knowledge about dN/dh and H_T makes this problem challenging. Therefore, in the following section, an assessment of $\Delta(dN/dh)$ and H_T will be made using the other radar measurements—power variations with elevation.

3. Extracting dN/dh information from returned power

a. Concept of a pointlike target

Using the returned power (P) of a point target at multiple low antenna-scanning elevations (θ) takes advantage of the radar antenna beam pattern. The linear antenna gain function can be approximated by a Gaussian shape (Probert-Jones 1962). When the radar scans across a point target, the relative returned power at each antenna elevation, $P(\theta)$, with respect to the maximum power return (P_o) at the representative elevation (θ_o) should mimic the radar beam pattern such that

$$\frac{P(\theta)}{P_o} = \exp\left[\frac{-(\theta-\theta_o)^2}{2\sigma^2}\right]. \tag{10}$$

The standard deviation (σ) of the Gaussian distribution is related to the 6-dB antenna beamwidth equal to $2\sigma\sqrt{2\ln 4}$. The θ_o is the one that results in the center of the main beam traveling from the radar to the given ground target. The received power changes at a rate that depends on the relative angle off the center of the main beam ($\theta-\theta_o$). Figure 4a illustrates that the observed reflectivity from a target at successive scanning elevations can be fitted with the known radar beam pattern. The θ_o associated with the target's position is consequently identified as the maximum returned power, which occurs at 0.14° for the target considered in Fig. 4a.

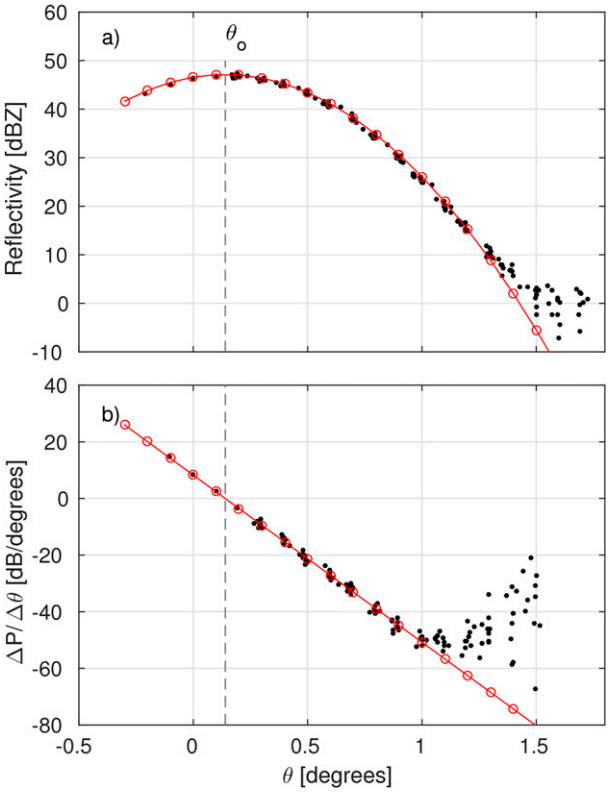

FIG. 4. (a) Power pattern of a selected ground target as a function of antenna elevation. The target is located at the 240° azimuth and the 228th gate. Black dots show the reflectivity measured at multiple antenna elevations. These measurements are fitted with a Gaussian function of the width of the antenna beam (red line with circles). The noisy reflectivity near $\theta = 1.5°$ is due to the null of the antenna. This particular example was chosen because it is a rare case where the center of the main beam is observed; for most targets, only one side of the main lobe is observed. (b) First-order derivative of the reflectivity pattern in (a) with respect to elevation θ showing the linearity of $\Delta P/\Delta\theta$ with θ. The red line illustrates the results of a linear regression through the data assuming a slope derived from the Gaussian antenna beam pattern as in (a).

A point target can be identified by fitting the received powers at successive antenna elevations $P(\theta)$ with the radar beam pattern. This process is identical but reversed from past studies that used point targets to determine antenna properties (e.g., Rinehart and Tuttle 1981; Rinehart and Frush 1983). However, direct interpretation of returned power is complicated due to the unknown size, number, position, etc., of ground target(s) within a resolved volume. Thus, targets with $P(\theta)$ similar to the antenna pattern indicate only their "pointlike" behavior, as opposed to more complex patterns that would be expected from extended targets.

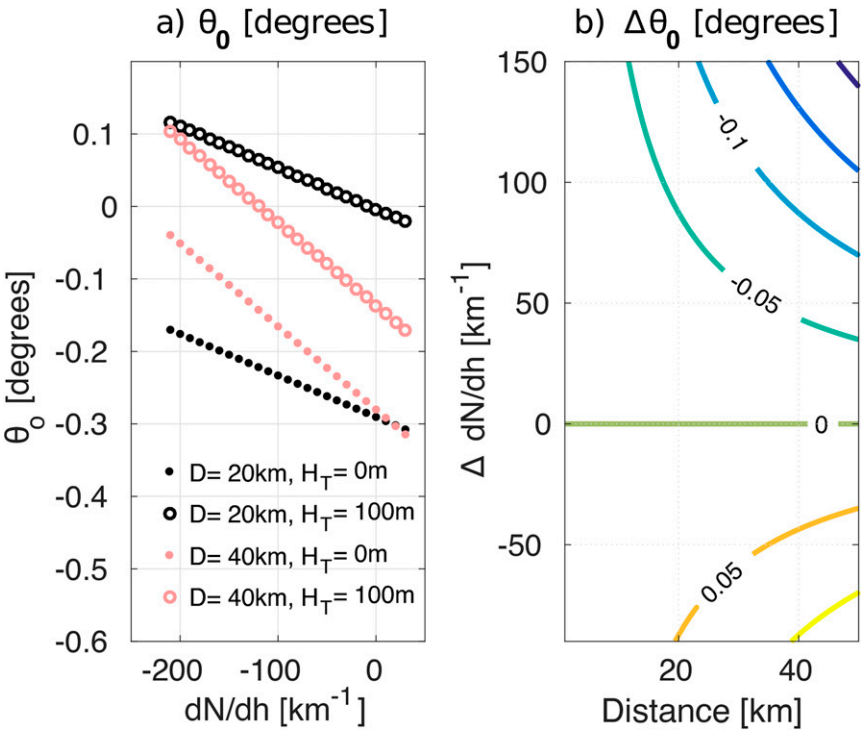

FIG. 5. (a) Representative elevation θ_o (°) of ground targets at different distance D and height H_T as a function of dN/dh conditions. At closer ranges, θ_o is more sensitive to differences in target heights; at farther ranges, it decreases more with changes in dN/dh. (b) Variation of the representative elevation $\Delta\theta_o$ as a function of D and $\Delta(dN/dh)$.

A simpler method is further proposed to effectively investigate the pointlike property of targets based on the parabolic shape of $P(\theta)$ on a logarithmic scale. The first-order derivative of the logarithmic $P(\theta)$ function within the main beam is linear with a constant slope determined by the antenna beamwidth (Fig. 4b). The power difference between two elevation angles decreases linearly with averaged antenna elevations. Meanwhile, this linear fitting method can be used to determine θ_o where the power difference is zero. Note that 1) the linear approximation is valid only in the main lobe, and 2) any deviation from the expected slope in the main beam indicates that the targets are either point targets with saturated power or not pointlike targets.

b. Using echo power at multiple elevations

How can the power measurements of pointlike targets be applied to retrieve further information for improving refractivity retrieval? The representative elevation θ_o links the observed power and the behavior of the beam path from the radar to the target under a particular atmospheric propagation condition. It is a function of the location of the targets (D, H_T) and the vertical gradient of refractivity (dN/dh):

$$\theta_o\left(D, H_T, \frac{dN}{dh}\right) = \tan^{-1}\left\{\frac{1}{\sin\left(\frac{D}{a_e}\right)} \times \left[\cos\left(\frac{D}{a_e}\right) - \frac{a_e}{H_T + a_e - H_R}\right]\right\}, \quad (11)$$

where $a_e = a/[1 + (a/10^6)(dN/dh)]$ is the effective earth's radius associated with a given dN/dh.

Figure 5a shows the varying θ_o of targets at different D and H_T under a series of dN/dh conditions. For a given pointlike target, θ_o decreases with increasing dN/dh. At closer range, θ_o is more sensitive to differences in H_T, with changes in θ_o caused by varying dN/dh being small compared to those associated with varying heights. But at further ranges, θ_o is more sensitive to changes in dN/dh. Furthermore, the variation of θ_o at given $\Delta(dN/dh)$ depends only on D, not on H_T. Hence, Fig. 5b shows the change of θ_o as a function of $\Delta(dN/dh)$ and D, and it illustrates that θ_o changes more at greater distances. Although θ_o provides constraints on H_T and dN/dh, it is still an underdetermined problem. Are there any glimmers of hope to estimate these two variables or at least one of them?

1) ESTIMATING H_T

Based on the concept of the radar beam height equation in Doviak and Zrnić (1993), the power-weighted height of a point target can be estimated as

$$H_T = a_e \left[\frac{\cos(\theta_o)}{\cos\left(\theta_o + \frac{D}{a_e}\right)} - 1 \right], \tag{12}$$

where H_T can be obtained with known D and observed θ_o, but dN/dh and a_e are still unknown. The dN/dh is more predictable in a well-mixed lower boundary layer during the afternoon, and it is expected to be between -40 and $-20\,\mathrm{km}^{-1}$. For example, by using (12), if targets are located at 20 and 40 km from the radar, then a $10\,\mathrm{km}^{-1}$ uncertainty of dN/dh would lead to a 2- and 8-m error in H_T, respectively, and a 0.01° observation bias in θ_o causes a 3.5- and 7-m error in H_T, respectively. Thus, the estimation of H_T will have higher uncertainty at farther distances. A very accurate θ_o to a hundredth of a degree is required for height estimation. In reality, there are only a few targets for which this method can be used because the returned powers of most targets at lower elevations and close range are saturated, leading to wrong θ_o estimates.

2) ESTIMATING dN/dh

If H_T can be determined well enough, then dN/dh may be obtained from the temporal variation of θ_o of selected targets based on (11). Although H_T is unknown, it can be estimated with reasonable accuracy by using terrain height and adding an estimated average height above the terrain. In rural areas, most of the ground targets are usually at a few meters above the terrain. Experience suggests that the mean and the standard deviation of target heights above the terrain is about 10 m (Park and Fabry 2010) and maybe twice that in urban areas away from downtown cores. Therefore, terrain provides useful information to approximate the relative H_T variation among ground targets. Moreover, a sensitivity test of uncertainty of H_T and θ_o on dN/dh estimation is examined based on (11) and (12). A 10-m uncertainty on H_T causes a dN/dh estimation error of $12.5\,\mathrm{km}^{-1}$ at 40 km but a $50.6\,\mathrm{km}^{-1}$ error at 20 km in range. A 0.01 degree uncertainty in θ_o results in a 17.5 and $8.7\,\mathrm{km}^{-1}$ error in dN/dh estimation for a target at 20 and 40 km, respectively. High accuracy of observed θ_o is still required. Targets at far ranges remaining well within the main lobe of the antenna under all propagation conditions are hence optimal for estimating dN/dh because more variation of θ_o occurs at far range than at close range for the same $\Delta(dN/dh)$ (Fig. 5a).

3) NORMALIZED dN/dh FROM $P(\theta_2) - P(\theta_1)$

For operational radars, it is not practical to execute many low-elevation scans to obtain θ_o for dN/dh estimation. Hence, an alternative algorithm using only two low elevations is developed. The θ_o of a pointlike ground target in the main lobe can be estimated from the observed power difference (dB) at two elevations, $\Delta P = P(\theta_2) - P(\theta_1)$ given $\theta_2 > \theta_1$, as

$$\theta_o = \frac{2\sigma^2 \ln 10^{\Delta P/10} + \theta_2^2 - \theta_1^2}{2(\theta_2 - \theta_1)}. \tag{13}$$

For a given pointlike target, θ_o decreases linearly with increasing dN/dh (Fig. 5a). Based on the linearity of the first-order derivative of $P(\theta)$, ΔP changes linearly with θ_o and dN/dh. Thus, ΔP can be used to retrieve dN/dh quantitatively.

Nevertheless, ΔP is not identical for different ground targets even under a given dN/dh, as it also depends on H_T and D. An assumption of spatially constant dN/dh is made. For each target, the two extreme opposite ΔP are selected as references, $\Delta P_{dN/dh_{\max}}$ and $\Delta P_{dN/dh_{\min}}$ occurring at the maximum and the minimum dN/dh, respectively, during a time period of few days. Thus, the relative dN/dh change among targets during that time period can be normalized as

$$\frac{\frac{dN}{dh} - \frac{dN}{dh}_{\max}}{\frac{dN}{dh}_{\min} - \frac{dN}{dh}_{\max}} = \frac{\Delta P - \Delta P_{dN/dh_{\max}}}{\Delta P_{dN/dh_{\min}} - \Delta P_{dN/dh_{\max}}}. \tag{14}$$

The normalized dN/dh can be estimated by the power difference between the two lowest elevations of surveillance scans for operational radars. Consequently, by combining with the two different dN/dh values obtained from the calibration scans, the dN/dh value in real time can be readily available. Given that (9) uses true dN/dh, the temporal qualitative variation of normalized dN/dh derived from (14) still provides valuable information as a quick quality check index of retrieved refractivity associated with dN/dh.

4. Validation of dN/dh retrievals

a. Data

The new method of dN/dh estimation is applied to the National Center for Atmospheric Research (NCAR)

S-band radar (S-Pol) in Colorado. The estimated dN/dh by the radar is compared with the in situ observation from the Boulder Atmospheric Observatory (BAO) tower close to the S-Pol radar (Fig. 6). The center of the antenna of the S-Pol radar is about 12 m above the ground and the antenna beamwidth is 0.92°. Two special scanning strategies were conducted in this experiment. The first was to obtain the properties of ground targets and to select suitable pointlike targets. Successive low-elevation scans from −0.2° to 2° in 0.1° intervals were collected on a clear windy afternoon from 1907 to 2242 UTC 27 January 2015. The second stage aimed to capture the signal of diurnal dN/dh variation lasting for a few clear days from 2137 UTC 20 March to 1427 UTC 23 March 2015. Scans at the following six elevations were collected: 0°, 0.4°, 0.6°, 0.8°, 1.0°, and 1.2°.

Ground targets are first distinguished from weather and other signals using the following criteria: The average returned power at 0.3° and 0.6° elevations during the first experiment are higher than 25 dBZ, and the standard deviation of the power at each elevation over the 4 h of the first data experiment is less than 1.5 dB to ensure the stability of power returns; the average clutter phase alignment (CPA; Hubbert et al. 2009) is higher than 0.85 and its standard deviation is smaller than 0.03. High CPA implies that phase and power are consistent within the resolved volume. In addition, the pointlike nature of the target is checked by fitting a line through the first-order derivative of $P(\theta)$ within the main beam and comparing it with the slope expected from the antenna beam pattern: The slope associated with the S-Pol radar antenna is -56.9 (dB deg^{-2}), and the slope of the targets should be within the range -56.9 ± 3 (dB deg^{-2}) to be declared pointlike. The number of ground targets in the selected area (210°–240° in azimuth, 20–40 km) meeting the criterion of having stable power returns is 315, 75 of those further meeting the pointlike target criterion. The final selected pointlike targets are generally at elevations less than 300 m above the radar (Fig. 6).

The BAO tower (NOAA 2015) collects near-surface atmospheric basic variables: temperature, relative humidity, and wind every minute at 10-, 100-, and 300-m height above the ground. Only surface pressure is measured, and the pressure at other elevations is derived from the hydrostatic equation. The refractivity value at each level is calculated based on (1). The vertical profile of refractivity between different heights is obtained as an in situ observation for comparison.

b. dN/dh estimation from selected targets

An example of a selected pointlike target illustrates how to use echo powers to estimate dN/dh (Figs. 7 and 8).

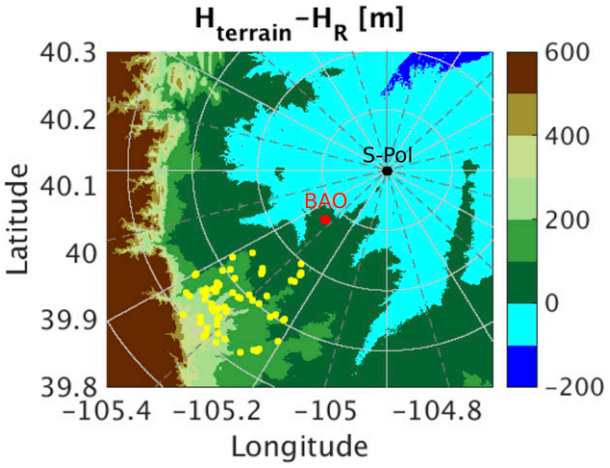

FIG. 6. Map of height difference (m) between the terrain and the S-Pol radar (located in the center of the range rings). The gray lines show the azimuth angles at 30° intervals relative to the S-Pol radar, and the rings are in 10-km range intervals away from the radar. The BAO tower is shown as a red dot at 229.5° in azimuth and 12.56 km away from the radar. The yellow dots are the selected ground targets for dN/dh estimation.

Figure 7 shows the variation of $P(\theta)$ and the first derivative of $P(\theta)$ for nearly 3 days in the second experiment. As dN/dh becomes more negative, the patterns of $P(\theta)$ and θ_o shift to a higher elevation. This occurs because the beam path at a given antenna elevation θ bends more toward the ground under superrefraction conditions; thus, it requires a beam with a higher θ_o than under normal propagation conditions to reach the target. The time series of $P(\theta)$, ΔP, and θ_o (Figs. 8a–c) show similar diurnal variations: decreasing during the day but increasing during the night. A sudden drop of θ_o in the nighttime (28th–35th h) occurs due to a frontal passage (Fig. 8c). Finally, ΔP can be normalized between 0 and 1, corresponding to the minimum and maximum of dN/dh, respectively, during this time period (Fig. 8d). The observed returned reflectivity, ΔP, and θ_o are all negatively correlated with dN/dh. The relative dN/dh physically represents the near-surface mixing conditions: relatively higher dN/dh occurring during daytime due to the well-mixed boundary layer. In addition, this normalized dN/dh helps quickly integrate the $\Delta(dN/dh)$ from many selected targets at different heights and distance even although their ΔP and θ_o are different.

An ensemble of ground targets is used to estimate an average dN/dh. Finding more than one pointlike target increases confidence in the dN/dh estimation, because it might reduce the uncertainties in guessing of H_T and biasing estimated θ_o. Figure 9a illustrates the similar diurnal trend of θ_o among selected targets. The different magnitudes of θ_o are due to the different distances and

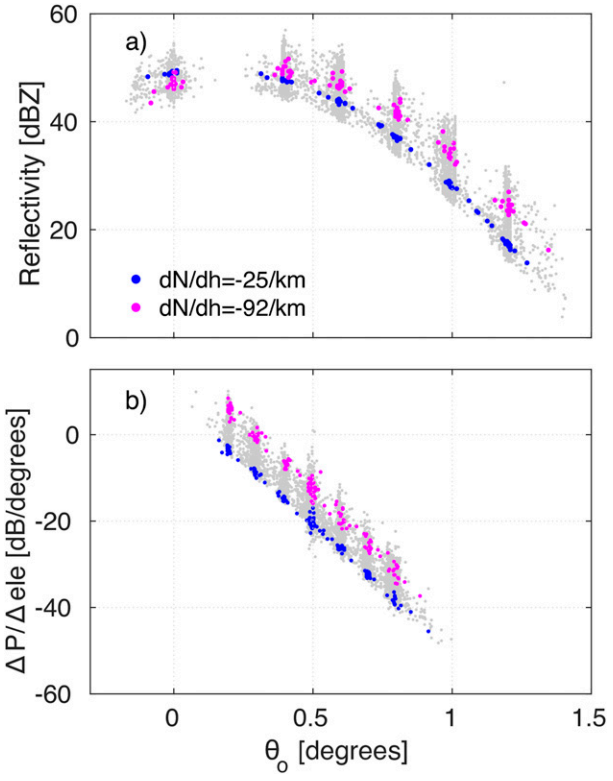

FIG. 7. Returned power variation of the selected target of Fig. 4 for 3 days. (a) Reflectivity observed at multiple radar elevations under a variety of conditions (gray dots). The colored dots highlight two specific dN/dh conditions: one in normal condition ($dN/dh = -25\,\mathrm{km}^{-1}$, blue) and one in superrefraction condition ($dN/dh = -92\,\mathrm{km}^{-1}$, magenta). (b) First-order derivative of power vs antenna elevation. Colored dots are as in (a).

heights of individual ground targets. Based on the linear relationship between θ_o and dN/dh, the average observed θ_o from an ensemble of targets, $\overline{\theta_o}_{\mathrm{Targets}}$, is able to represent the average dN/dh. Then, $\overline{\theta_o}(dN/dh)_{\mathrm{guess}}$, the average θ_o from the selected targets under a wide range of dN/dh conditions, is calculated based on (11). The target heights here are approximated as the terrain height plus an assumed target height of 10 m above the surface, that is, $H_{T\mathrm{guess}} = H_{\mathrm{terrain}} + 10$ m. The estimated dN/dh from the radar and targets, dN/dh_{Radar}, is determined from the minimum absolute difference between $\overline{\theta_o}_{\mathrm{Targets}}$ and $\overline{\theta_o}(dN/dh)_{\mathrm{guess}}$. Note that a mean bias in target heights of 5 m in this case will lead to a relatively small dN/dh estimation bias of 5–10 km^{-1}.

c. Radar–tower comparison of dN/dh

The estimated dN/dh_{Radar} is consistent with the dN/dh measurement between 10 and 100 m of the BAO tower (Fig. 9b), although there is a difference of dN/dh in magnitude between these two datasets. The correlation coefficient between the estimated and observed dN/dh is above 0.8 (Fig. 10). Moreover, there is a correlation coefficient greater than 0.9 between dN/dh from the BAO tower and relative dN/dh derived from ΔP for any combination of antenna elevation angles within the antenna main beam.

The discrepancy of dN/dh estimation between the radar estimation and the BAO tower requires further discussions. The first point to consider is the data quality of measured power of targets. The power of a ground target at a given elevation usually fluctuates (Fig. 8a), which produces noisier ΔP and more uncertainties in θ_o. Fluctuations in returned power of ground targets occur due to a variety of causes, from scintillation to slight changes in target shape. Then, the atmosphere is not horizontally homogeneous. Furthermore, some radars might have a position pointing bias and the accuracy of the reading of the antenna elevations needs to be considered. Though the difference in elevation might be small, it can lead to a large difference in the power considering the parabolic shape of the antenna pattern, and it may lower the accuracy of θ_o estimations to which dN/dh estimations are sensitive. Here, the average difference θ_o between the radar estimation and the known dN/dh from the BAO tower is calculated to estimate the bias in antenna elevation reporting. This calculation suggests a pointing bias of approximated 0.03° that can be used to obtain a new corrected dN/dh (light blue line in Fig. 9b) that better matches observations. But overall, the diurnal trend still dominates and can be retrieved despite all other sources of power fluctuations.

In addition, differences in measurement representativeness might explain the discrepancies in dN/dh. The BAO tower is a single-point observation, but the estimation from ground targets is the averaged result of a nearby area. Furthermore, the representative heights are different: the dN/dh from the BAO tower is the refractivity difference between 10 and 100 m above the ground, but the dN/dh radar estimates are much closer to the ground. In particular, the large nighttime negative dN/dh might appear earlier and be stronger in layers close to the ground than in the higher tower observations, due to the gradual buildup of the inversion. Furthermore, dN/dh has more variability at night as previously shown by in situ observation or radar estimations (Fig. 9).

Finally, the power of a given pixel is not only affected by the beam propagation condition (dN/dh) but also by some partial beam blockage by ground obstacles in front of the targets and the complexity (number, combination) of the ground targets within the resolved volume. In addition, interference between different elements of a complex

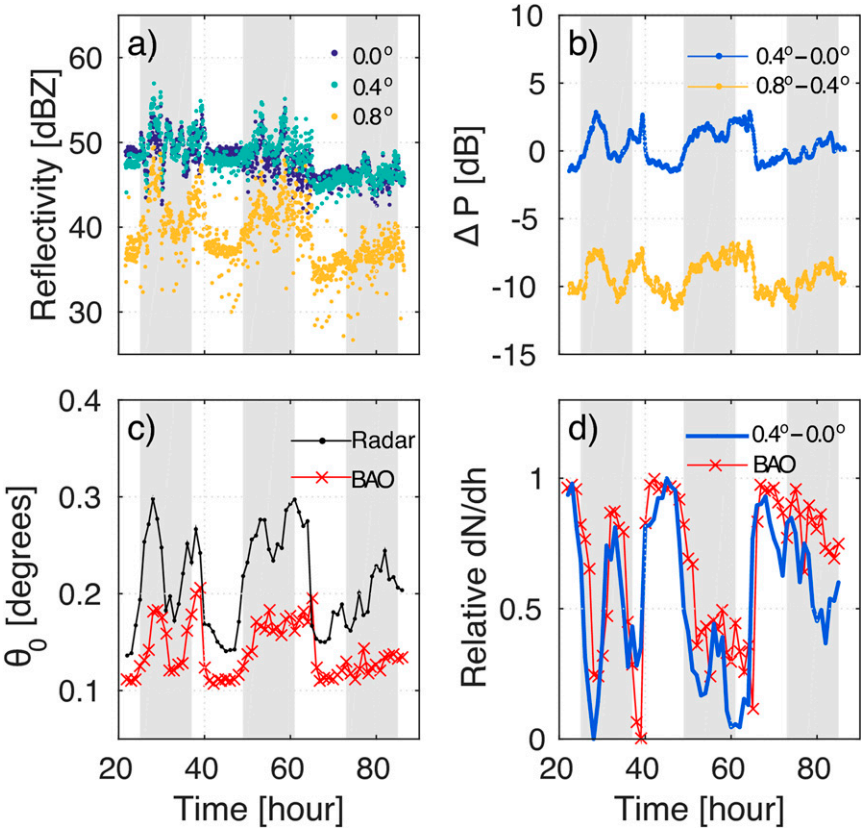

FIG. 8. Illustrations of how dN/dh is retrieved for the target selected in Fig. 4. (a) Temporal series of power returned (dBZ) from the target for the radar antenna elevation angles at 0°, 0.4°, and 0.8°. The gray shading indicates the nighttime after sunset until the next sunrise. (b) Power difference ΔP between two elevations in time smoothed using a 1-h running average. The blue line shows $\Delta P_1 = P_{0.4^\circ} - P_{0.0^\circ}$ and the yellow line is $\Delta P_2 = P_{0.8^\circ} - P_{0.4^\circ}$. (c) Representative target-center elevation θ_o obtained from the radar and the BAO tower based on (13). (d) Normalized dN/dh in this experiment period ranging between one (the maximum dN/dh) and zero (the minimum dN/dh). The blue line is derived from ΔP_1, while the red line shows the normalized dN/dh between 10 and 100 m derived using data from the BAO tower.

target could be mainly destructive under some dN/dh conditions, leading to an unexpectedly decreasing returned power during superrefraction or ducting conditions.

In summary, power measurements at successive low elevations can be used to qualitatively describe the diurnal dN/dh variation, which is key to improving refractivity retrieval based on (9). Moreover, the promising result of dN/dh estimation might be applied to operational radars and provide real-time information on near-surface beam propagation conditions, which affects the data quality of quantitative precipitation estimation, ground clutter elimination, and other applications.

5. Concluding remarks

Variable target heights and changing dN/dh affect and bias refractivity retrievals obtained by radar: first, targets are at different heights, and their information is harder to combine; then, propagation changes, as a result of which the trajectory of the radar beam to the target changes, along with refractivity sampled along the way. To mitigate these issues, we must seek to retrieve a map of refractivity at a constant height above terrain. Achieving this requires first obtaining a 2D refractivity map at the height of the radar and then combining it with an altitude correction that depends on target heights and dN/dh. Enabling this vision forced us to rethink the information that can be obtained by radar for each target.

Using a theoretical reanalysis of the equation of the returned phase of a target, the representativeness of the measured phase and of the retrieved refractivity are clarified, and the systematic refractivity biases are quantified and shown to be related to the effect of H_T

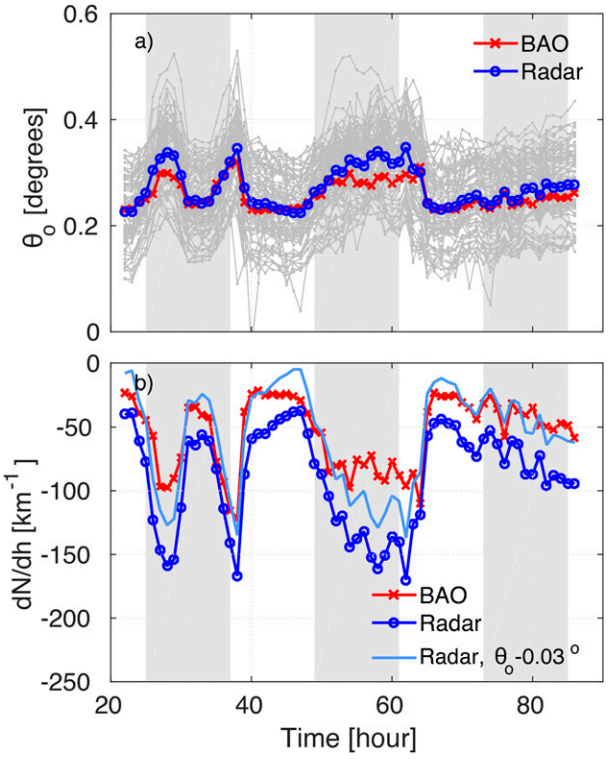

FIG. 9. (a) Time series of θ_o from the selected pointlike targets shown in gray lines. The blue line with circles is the hourly average θ_o among ground targets. The red line with crosses is the average θ_o calculated based on the dN/dh from the BAO tower, as well as D and H_T of selected targets. The gray shaded periods represent the nighttime as mentioned in Fig. 8. (b) Time evolution of dN/dh of the BAO tower (red line) and of the radar estimation (blue line with circles). The light blue line shows the corrected radar estimation dN/dh considering a 0.03° pointing angle correction of the antenna.

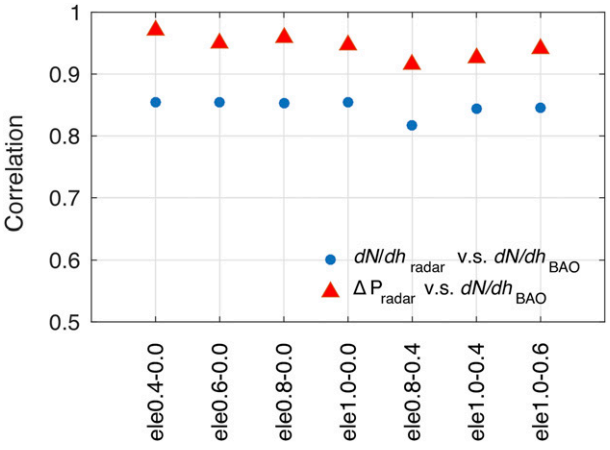

FIG. 10. Correlation coefficients between the time series of dN/dh estimated from the BAO tower and derived from power differences at given antenna elevations of S-Pol (blue dots). Red triangles show the correlation between the relative dN/dh of S-Pol and of the BAO tower.

and of the changing trajectory with changes in dN/dh. Temporal biases of N over the whole domain may arise as a result of the evolving dN/dh associated with the near-surface layer mixing conditions; biases of refractivity over very short pathlengths occur due to the variability of heights of ground targets. Taking these biases and errors into account can also help reduce the noisiness of phase measurements and also help mitigate the $\Delta\phi$ unfolding problem. Despite these improvements, some noise in the $\Delta\phi$ field remains due to unknown target heights and the intrinsic complexity of ground targets. As a result, it is still necessary to smooth or do regression on the corrected $\Delta\phi$ field with a reasonable window in order to estimate the gradient of $\Delta\phi$ and the small-scale refractivity variations.

A practical method to estimate dN/dh and H_T is then proposed. It is based on the concept that the power returned by a point target at successive antenna elevations can be described by the antenna beam pattern. Since both the power and phase of a stationary target record the evolving atmospheric conditions that the radar beam travels through, the difference in returned power at two given elevations and the elevation of peak power of selected pointlike targets evolve linearly with dN/dh. An ensemble of pointlike targets is used to estimate an average dN/dh, which shows promising and consistent trends when compared with the in situ observation of the BAO tower. Information on dN/dh might be obtained from numerical weather model output or in situ tower observation. However, there are often quantitative differences in dN/dh between model output and in situ data that might be related to uncertainties in boundary layer processes in model simulations. In situ tower observations are helpful, but they are not readily available for most radar sites. Hence, the new method of dN/dh estimation is encouraged to be applied to operational radars. Furthermore, a theoretical method to estimate the power-weighted height of the target is developed, but there are some practical problems in obtaining the H_T of all ground targets. Although the height of most targets remains unknown and challenging to obtain, terrain can be used as a useful proxy to describe the height difference between targets. In addition, the assigned height above the terrain should be set reasonably and consider the practical conditions of target heights; here, 10 m above the terrain is used for rural areas.

Using this new theoretical basis, the magnitude of systematic biases in refractivity retrievals can be reduced by including the effects of terrain and target height. To make this possible, a new step-by-step processing to retrieve N based on these results should be as follows: 1) determine H_T based on the terrain;

2) measure N_{ref} and $(dN/dh)_{ref}$ in known N and dN/dh conditions; 3) in real time, use echo power at different elevations to determine dN/dh; and, 4) use (9) to retrieve N at a desired altitude.

Acknowledgments. The authors thank Dr. Mike Dixon for helping to collect special scans with the NCAR S-Pol radar. We also used in situ BAO observation provided by the NOAA/OAR/ESRL PSD, and we thank NOAA for its generosity. We also thank Dr. Isztar Zawadzki for the many fruitful discussions and Mr. Jonathan Vogel for assistance with the English grammar. This work was made possible thanks to the support from the Natural Sciences and Engineering Research Council of Canada (NSERC).

REFERENCES

Besson, L., C. Boudjabi, O. Caumont, and J. Parent du Chatelet, 2012: Links between weather phenomena and characteristics of refractivity measured by precipitation radar. *Bound.-Layer Meteor.*, **143**, 77–95, doi:10.1007/s10546-011-9656-7.

Bodine, D., and Coauthors, 2011: Understanding radar refractivity: Sources of uncertainty. *J. Appl. Meteor. Climatol.*, **50**, 2543–2560, doi:10.1175/2011JAMC2648.1.

Buban, M. S., C. L. Ziegler, E. N. Rasmussen, and Y. P. Richardson, 2007: The dryline on 22 May 2002 during IHOP: Ground-radar and in situ data analyses of the dryline and boundary layer evolution. *Mon. Wea. Rev.*, **135**, 2473–2505, doi:10.1175/MWR3453.1.

Caumont, O., A. Foray, L. Besson, and J. Parent du Châtelet, 2013: An observation operator for radar refractivity change: Comparison of observations and convective-scale simulations. *Bound.-Layer Meteor.*, **148**, 379–397, doi:10.1007/s10546-013-9820-3.

Chen, F., and Coauthors, 2007: Description and evaluation of the characteristics of the NCAR high-resolution land data assimilation system. *J. Appl. Meteor. Climatol.*, **46**, 694–713, doi:10.1175/JAM2463.1.

Crook, N. A., 1996: Sensitivity of moist convection forced by boundary layer processes to low-level thermodynamic fields. *Mon. Wea. Rev.*, **124**, 1767–1785, doi:10.1175/1520-0493(1996)124<1767:SOMCFB>2.0.CO;2.

Dabberdt, W. F., and T. W. Schlatter, 1996: Research opportunities from emerging atmospheric observing and modeling capabilities. *Bull. Amer. Meteor. Soc.*, **77**, 305–323, doi:10.1175/1520-0477(1996)077<0305:ROFEAO>2.0.CO;2.

Doviak, R. J., and D. S. Zrnić, 1993: Electromagnetic waves and propagation. *Doppler Radar and Weather Observations*. 2nd ed. Academic Press, 10–29, doi:10.1016/B978-0-12-221422-6.50007-3.

Emanuel, K., and Coauthors, 1995: Report of the first prospectus development team of the U.S. weather research program to NOAA and the NSF. *Bull. Amer. Meteor. Soc.*, **76**, 1194–1208.

Fabry, F., 2004: Meteorological value of ground target measurements by radar. *J. Atmos. Oceanic Technol.*, **21**, 560–573, doi:10.1175/1520-0426(2004)021<0560:MVOGTM>2.0.CO;2.

——, 2006: The spatial variability of moisture in the boundary layer and its effect on convection initiation: Project-long characterization. *Mon. Wea. Rev.*, **134**, 79–91, doi:10.1175/MWR3055.1.

——, and J. Sun, 2010: For how long should what data be assimilated for the mesoscale forecasting of convection and why? Part I: On the propagation of initial condition errors and their implications for data assimilation. *Mon. Wea. Rev.*, **138**, 242–255, doi:10.1175/2009MWR2883.1.

——, C. Frush, I. Zawadzki, and A. Kilambi, 1997: On the extraction of near-surface index of refraction using radar phase measurements from ground targets. *J. Atmos. Oceanic Technol.*, **14**, 978–987, doi:10.1175/1520-0426(1997)014<0978:OTEONS>2.0.CO;2.

Fritz, J., and V. Chandrasekar, 2009: Implementation and analysis of networked radar refractivity retrieval. *J. Atmos. Oceanic Technol.*, **26**, 2123–2135, doi:10.1175/2009JTECHA1182.1.

Gasperoni, N. A., M. Xue, R. D. Palmer, and J. Gao, 2013: Sensitivity of convective initiation prediction to near-surface moisture when assimilating radar refractivity: Impact tests using OSSEs. *J. Atmos. Oceanic Technol.*, **30**, 2281–2302, doi:10.1175/JTECH-D-12-00038.1.

Hanley, K. E., D. J. Kirshbaum, S. E. Belcher, N. M. Roberts, and G. Leoncini, 2011: Ensemble predictability of an isolated mountain thunderstorm in a high-resolution model. *Quart. J. Roy. Meteor. Soc.*, **137**, 2124–2137, doi:10.1002/qj.877.

Hao, Y., D. Goeckel, R. Janaswamy, and S. Frasier, 2006: Surface refractive index field estimation from multiple radars. *Radio Sci.*, **41**, RS3002, doi:10.1029/2005RS003288.

Heinselman, P. L., B. L. Cheong, R. D. Palmer, D. Bodine, and K. Hondl, 2009: Radar refractivity retrievals in Oklahoma: Insights into operational benefits and limitations. *Wea. Forecasting*, **24**, 1345–1361, doi:10.1175/2009WAF2222256.1.

Hubbert, J. C., M. Dixon, S. M. Ellis, and G. Meymaris, 2009: Weather radar ground clutter. Part I: Identification, modeling, and simulation. *J. Atmos. Oceanic Technol.*, **26**, 1165–1180, doi:10.1175/2009JTECHA1159.1.

Koch, S. E., W. Feltz, F. Fabry, M. Pagowski, B. Geerts, K. M. Bedka, D. O. Miller, and J. W. Wilson, 2008: Turbulent mixing processes in atmospheric bores and solitary waves deduced from profiling systems and numerical simulation. *Mon. Wea. Rev.*, **136**, 1373–1400, doi:10.1175/2007MWR2252.1.

Montmerle, T., A. Caya, and I. Zawadzki, 2002: Short-term numerical forecasting of a shallow storms complex using bistatic and single-Doppler radar data. *Wea. Forecasting*, **17**, 1211–1225, doi:10.1175/1520-0434(2002)017<1211:STNFOA>2.0.CO;2.

Nicol, J. C., and A. J. Illingworth, 2013: The effect of phase-correlated returns and spatial smoothing on the accuracy of radar refractivity retrievals. *J. Atmos. Oceanic Technol.*, **30**, 22–39, doi:10.1175/JTECH-D-12-00077.1.

——, ——, T. Darlington, and M. Kitchen, 2013: Quantifying errors due to frequency changes and target location uncertainty for radar refractivity retrievals. *J. Atmos. Oceanic Technol.*, **30**, 2006–2024, doi:10.1175/JTECH-D-12-00118.1.

——, ——, and K. Bartholomew, 2014: The potential of 1 h refractivity changes from an operational C-band magnetron-based radar for numerical weather prediction validation and data assimilation. *Quart. J. Roy. Meteor. Soc.*, **140**, 1209–1218, doi:10.1002/qj.2223.

NOAA, 2015: BAO tower data. Accessed 20 April 2016. [Available online at http://www.esrl.noaa.gov/psd/technology/bao/.]

Parent du Chatelet, J., C. Boudjabi, L. Besson, and O. Caumont, 2012: Errors caused by long-term drifts of magnetron frequencies for refractivity measurement with a radar: Theoretical formulation and initial validation. *J. Atmos. Oceanic Technol.*, **29**, 1428–1434, doi:10.1175/JTECH-D-12-00070.1.

Park, S., and F. Fabry, 2010: Simulation and interpretation of the phase data used by the radar refractivity retrieval algorithm.

J. Atmos. Oceanic Technol., **27**, 1286–1301, doi:10.1175/2010JTECHA1393.1.

Probert-Jones, J. R., 1962: The radar equation in meteorology. *Quart. J. Roy. Meteor. Soc.*, **88**, 485–495, doi:10.1002/qj.49708837810.

Rinehart, R. E., and J. D. Tuttle, 1981: A technique for determining antenna beam patterns using a ground target. Preprints, *20th Conf. on Radar Meteorology*, Boston, MA, Amer. Meteor. Soc., 672–675.

——, and C. L. Frush, 1983: Comparison of antenna beam patterns obtained from near-field test measurements and ground target scans. Preprints, *21st Conf. on Radar Meteorology*, Edmonton, Alberta, Canada, Amer. Meteor. Soc., 291–295.

Roberts, R. D., and Coauthors, 2008: REFRACTT 2006: Real-time retrieval of high-resolution, low-level moisture fields from operational NEXRAD and research radars. *Bull. Amer. Meteor. Soc.*, **89**, 1535–1548, doi:10.1175/2008BAMS2412.1.

Sherwood, S. C., W. Ingram, Y. Tsushima, M. Satoh, M. Roberts, P. L. Vidale, and P. A. O'Gorman, 2010: Relative humidity changes in a warmer climate. *J. Geophys. Res.*, **115**, doi:10.1029/2009JD012585.

Smith, E. K., and S. Weintraub, 1953: The constants in the equation for atmospheric refractive index at radio frequencies. *Proc. IRE*, **41**, 1035–1037, doi:10.1109/JRPROC.1953.274297.

Sun, J., 2005: Convective-scale assimilation of radar data: Progress and challenges. *Quart. J. Roy. Meteor. Soc.*, **131**, 3439–3463, doi:10.1256/qj.05.149.

Wakimoto, R. M., and H. V. Murphey, 2010: Frontal and radar refractivity analyses of the dryline on 11 June 2002 during IHOP. *Mon. Wea. Rev.*, **138**, 228–241, doi:10.1175/2009MWR2991.1.

Weckwerth, T. M., 2000: The effect of small-scale moisture variability on thunderstorm initiation. *Mon. Wea. Rev.*, **128**, 4017–4030, doi:10.1175/1520-0493(2000)129<4017:TEOSSM>2.0.CO;2.

——, V. Wulfmeyer, R. M. Wakimoto, R. M. Hardesty, J. W. Wilson, and R. M. Banta, 1999: NCAR–NOAA lower-tropospheric water vapor workshop. *Bull. Amer. Meteor. Soc.*, **80**, 2339–2357, doi:10.1175/1520-0477(1999)080<2339:NNLTWV>2.0.CO;2.

——, C. R. Pettet, F. Fabry, S. J. Park, M. A. LeMone, and J. W. Wilson, 2005: Radar refractivity retrieval: Validation and application to short-term forecasting. *J. Appl. Meteor.*, **44**, 285–300, doi:10.1175/JAM-2204.1.

Zawadzki, I., E. Torlaschi, and R. Sauvageau, 1981: The relationship between mesoscale thermodynamic variables and convective precipitation. *J. Atmos. Sci.*, **38**, 1535–1540, doi:10.1175/1520-0469(1981)038<1535:TRBMTV>2.0.CO;2.